



**HAL**  
open science

## Annealing behaviour of nanocrystalline NiTi (50 at% Ni) alloy produced by high-pressure torsion

Reeti Singh, Sergiy Divinski, Harald Rösner, Egor Prokofyev, R. Z. Valiev,  
Gerhard Wilde

► **To cite this version:**

Reeti Singh, Sergiy Divinski, Harald Rösner, Egor Prokofyev, R. Z. Valiev, et al.. Annealing behaviour of nanocrystalline NiTi (50 at% Ni) alloy produced by high-pressure torsion. Philosophical Magazine, 2011, pp.1. 10.1080/14786435.2011.566228 . hal-00685380

**HAL Id: hal-00685380**

**<https://hal.science/hal-00685380>**

Submitted on 5 Apr 2012

**HAL** is a multi-disciplinary open access archive for the deposit and dissemination of scientific research documents, whether they are published or not. The documents may come from teaching and research institutions in France or abroad, or from public or private research centers.

L'archive ouverte pluridisciplinaire **HAL**, est destinée au dépôt et à la diffusion de documents scientifiques de niveau recherche, publiés ou non, émanant des établissements d'enseignement et de recherche français ou étrangers, des laboratoires publics ou privés.



**Annealing behaviour of nanocrystalline NiTi (50 at% Ni) alloy produced by high-pressure torsion**

Journal:	<i>Philosophical Magazine &amp; Philosophical Magazine Letters</i>
Manuscript ID:	TPHM-10-Jul-0329.R2
Journal Selection:	Philosophical Magazine
Date Submitted by the Author:	31-Jan-2011
Complete List of Authors:	Singh, Reeti; Universität Münster, Institute of Materials Physics Divinski, Sergiy; Universität Münster, Institute of Materials Physics Rösner, Harald; Universität Münster, Institute of Materials Physics Prokofyev, Egor; Ufa State Aviation University, Russia, Institute of Physics of Advanced Materials, Ufa Valiev, R. Z.; Ufa State Aviation University, Russia, Institute of Physics of Advanced Materials, Ufa Wilde, Gerhard; Universität Münster, Institute of Materials Physics
Keywords:	crystallization, grain boundaries, grain growth
Keywords (user supplied):	NiTi, Relaxation, Nanocrystalline

SCHOLARONE™  
Manuscripts

**Authors:**

(1) **Reeti Singh (corresponding author)**, Institut für Materialphysik, Westfälische Wilhelms-Universität Münster, Wilhelm-Klemm-Str. 10, 48149, Münster, Germany.

Email: [rsing\\_01@uni-muenster.de](mailto:rsing_01@uni-muenster.de)

Tel: +49 (0) 251 83 33578

Fax: +49 (0) 251 83 38346

(2) Sergiy Divinski, Institut für Materialphysik, Westfälische Wilhelms-Universität Münster, Wilhelm-Klemm-Str. 10, 48149, Münster, Germany.

Email: [divin@uni-muenster.de](mailto:divin@uni-muenster.de)

Tel: +49 (0) 251 83 39030

Fax: +49 (0) 251 83 38346

(3) Harald Rösner, Institut für Materialphysik, Westfälische Wilhelms-Universität Münster, Wilhelm-Klemm-Str. 10, 48149, Münster, Germany.

Email: [rosner@uni-muenster.de](mailto:rosner@uni-muenster.de)

Tel: +49 (0) 251 83 33573

Fax: +49 (0) 251 83 38346

(4) Egor A. Prokofyev, Institute of Physics of Advanced Materials, Ufa State Aviation University, 12 K. Marx Street, 450000 Ufa, Russian Federation.

Email: [egpro@mail.ru](mailto:egpro@mail.ru)

(5) Ruslan Z. Valiev, Institute of Physics of Advanced Materials, Ufa State Aviation University, 12 K. Marx Street, 450000 Ufa, Russian Federation.

Email: [rzvaliev@mail.rb.ru](mailto:rzvaliev@mail.rb.ru)

(6) Gerhard Wilde, Institut für Materialphysik, Westfälische Wilhelms-Universität Münster, Wilhelm-Klemm-Str. 10, 48149, Münster, Germany.

Email: [gwilde@uni-muenster.de](mailto:gwilde@uni-muenster.de)

Tel: +49(0) 251 83 33576

Fax: +49 (0) 251 83 38346

1  
2  
3  
4  
5  
6  
7  
8

## Annealing behaviour of nanocrystalline NiTi (50 at% Ni) alloy produced by high-pressure torsion

9  
10  
11  
12  
13  
14  
15  
16  
17  
18  
19

R. Singh<sup>1</sup>, H. Rösner<sup>1</sup>, E.A. Prokofyev<sup>2</sup>, R.Z. Valiev<sup>2</sup>, S.V. Divinski<sup>1</sup>, and G. Wilde<sup>1</sup>

<sup>1</sup>Institut für Materialphysik, Westfälische Wilhelms-Universität Münster, Wilhelm-  
Klemm-Str. 10, 48149, Münster, Germany

<sup>2</sup>Institute of Physics of Advanced Materials, Ufa State Aviation University, 12 K.  
Marx Street, 450000 Ufa, Russian Federation

### Abstract

20  
21  
22  
23  
24  
25  
26  
27  
28  
29  
30  
31  
32  
33  
34

An equiatomic nanocrystalline NiTi alloy, deformed by high-pressure torsion (HPT) was investigated. The as-prepared bulk NiTi alloy consists of both amorphous and nanocrystalline phases. Crystallization and structural changes during annealing were investigated by differential scanning calorimetry (DSC), X-ray diffraction (XRD) and transmission electron microscopy (TEM).

35  
36  
37  
38  
39  
40  
41  
42  
43  
44  
45  
46  
47  
48  
49  
50  
51  
52  
53  
54  
55  
56  
57  
58  
59  
60

The DSC thermograms and X-ray analyses reveal stress relaxation and partial crystallization below 500 K while grain growth of the nanocrystals occurs predominantly after heating to temperatures above 573 K. Along with the amorphous phase crystallization, a continuous growth of pre-existing nanocrystals that are retained after HPT was observed. The DSC signals observed during continuous heating experiments indicate an unusually large separation between the crystallization and the growth stages. A detailed analysis of the evolution of the enthalpy release upon annealing reveals reproducibly non-monotonous trends with annealing temperature that cannot be explained solely with nucleation and growth of crystalline volume fractions. Instead, the results can be rationalized by assuming a reverse amorphization process occurring during annealing at 523 K. This behavior, that also causes a large variation of the nanocrystals size after annealing at higher

1  
2  
3 temperatures, is discussed with respect to the nanoscale microstructural heterogeneity  
4  
5 after initial deformation processing.  
6  
7

8  
9 Keywords: NiTi, nanocrystalline, grain boundary, crystallization, relaxation

## 10 11 **1. Introduction**

12  
13  
14 The intermetallic compound NiTi also known as “Nitinol” with near equiatomic  
15  
16 composition of Ni and Ti has drawn much interest for its ability to be used, because of  
17  
18 its unique combination of thermal shape memory effect, superelasticity and good  
19  
20 damping [1-5]. Nitinol has many attractive service applications, particularly in the  
21  
22 field of biomedical technology such as, dental archwires, bone staples, endoscopic  
23  
24 instruments, stents and surgical retractors [6, 7].  
25  
26  
27

28  
29 The development of nanocrystalline Nitinol has been the subject of intensive research,  
30  
31 because fine grained or nanocrystalline material shows a variety of different and  
32  
33 improved properties compared to the conventional coarse-grained polycrystalline  
34  
35 material [8-16]. Recently, bulk nanocrystalline NiTi has attracted much interest as a  
36  
37 high-tech material, showing enhanced shape memory behavior and superelasticity  
38  
39 with ultra high recovery stress [9, 10]. HPT (high pressure torsion) is one of the  
40  
41 methods that allow obtaining nano-structured materials with new and unique  
42  
43 properties and small grain size [11]. Combining HPT and subsequent annealing  
44  
45 treatments one can tune the grain size and as a result the properties of the material can  
46  
47 be controlled [12-14]. One prominent example is the size effect that can significantly  
48  
49 shift the transformation from the cubic B2 high temperature phase to the monoclinic  
50  
51 B19' martensite; grains with a size less than 50 nm can even lead to the complete  
52  
53 suppression of the transformation [15, 16]. The kinetics of nucleation and grain growth  
54  
55 was measured by various experimental methods, such as differential scanning  
56  
57  
58  
59  
60

1  
2  
3 calorimetry (DSC), X-ray diffraction and in situ heating in the transmission electron  
4 microscope (TEM) on thin amorphous ribbons of NiTi and NiTiCu made by sputter  
5 deposition (SD) [17-20], melt spinning (MS) [21-24] and cold rolling [25, 26].  
6  
7 Crystallization of the amorphous thin ribbons leads to microcrystalline structures [18,  
8 19]. Contrary to these results, crystallization at low temperatures of the NiTi alloy  
9 made amorphous by HPT leads to nanocrystalline structures [12, 13, and 27].

10  
11  
12  
13  
14  
15  
16  
17  
18 Sergueeva et al. has investigated the structural changes in a NiTi alloy produced by  
19 HPT by in-situ heating in a transmission electron microscope (TEM) [12]. Very  
20 recently M. Peterlechner et al. also studied the crystallization of a HPT-processed  
21 NiTi alloy [27]. In the previous studies it has been reported by DSC and in-situ TEM  
22 that the crystallization of HPT deformed NiTi started at temperatures lower than  
23 473 K and finished at 673 K and there was a continuous increase in the crystalline  
24 volume fraction during heating as well as annealing. The present study is aimed to  
25 analyze if the crystallization and the growth transformations are truly monotonous in  
26 temperature and to investigate the crystallization and the related structure changes in  
27 detail during annealing of amorphous NiTi alloy produced by HPT, using DSC, XRD  
28 and TEM.  
29  
30  
31  
32  
33  
34  
35  
36  
37  
38  
39  
40  
41  
42

## 43 44 45 **2. Experimental details**

### 46 47 48 **2.1 Material**

49  
50  
51 In the present study, a NiTi alloy with a composition of Ni<sub>50.6</sub>Ti<sub>49.4</sub> in atomic percent  
52 was used. This material was provided by the Institute of Physics of Advanced  
53 Materials, Ufa State Aviation TU, Russia. The initial rod produced by Intrinsic  
54 Devices Inc. (USA) with a diameter of 21 mm was water quenched from 1073 K. The  
55  
56  
57  
58  
59  
60

discs cut from the quenched rod were subjected to HPT under a pressure of 5 GPa to a true logarithmic strain of 6, calculated by using the following formula:

$$\varepsilon = \ln\left(\frac{\theta r}{l}\right) \quad (1)$$

Where  $\varepsilon$  is the logarithmic strain,  $\theta$  is the rotation angle in radians,  $r$  is the radius and  $l$  is the thickness of the disc. The as-processed material is in the form of discs with diameters of 20 mm and thicknesses of about 0.8 mm. Discs of 4.5 mm (DSC & XRD measurements) and 3.0 mm (the TEM investigation) in diameter were cut from the as-processed disc by the spark erosion technique. The distance between the centers of the HPT deformed disc was for the DSC & XRD 7.75 mm and for the TEM samples 8.5 mm, respectively. Hence, according to Eq. (1), the averaged logarithmic strain in the DSC, XRD and TEM samples is 5.72 and 5.81, respectively.

## 2.2 Characterization

Calorimetric measurements were performed by differential scanning calorimetry (Diamond DSC, Perkin-Elmer) under Ar atmosphere. A consecutive of DSC scans was recorded with the same specimen with a heating rate 10 K/min with a continuously increasing final temperature in the range from 453 K to 723 K. One hour annealing at the final temperature followed each of these DSC scans. In detail, the data were collected according to the following scheme:

- (a) The as-prepared sample was heated to 453 K with a heating rate of 10 K/min followed by isothermal annealing for 1 h. After annealing, the sample was cooled down to 323 K using a cooling rate of 100 K/min.
- (b) Immediately after the first run, **the same sample** was heated to 523 K, isothermally held at 523 K for 1 h, and subsequently cooled down to 323 K.

1  
2  
3 (c) Similar runs were repeated by heating to and holding at consequently higher  
4 temperatures.  
5  
6

7  
8 (d) In this way, the same sample was heated to a consistently higher pre-selected  
9 temperature ranging from 453 K to 723 K followed by annealing for 1 h. The  
10 heating and cooling rates of 10 K/min and 100 K/min, respectively, were  
11 systematically used in each cycle.  
12  
13  
14  
15  
16

17  
18 In such a way, the thermally activated processes occurred during isothermal holding  
19 treatments could consistently be examined, avoiding uncertainties related to transient  
20 regimes during switching from heating to isothermal holding.  
21  
22  
23

24  
25 A second type of DSC scans was recorded to determine the heat release during  
26 annealing ( $\delta H$ ) at temperatures ranging from 453 K to 623 K by using different  
27 samples. The following measurements were performed:  
28  
29  
30  
31

32  
33 (1) One sample was continuously heated from 323 K to 723 K and the total heat  
34 release  $\delta H_{\text{total}}$  was measured, Fig. 1a. The reproducibility of the signal was  
35 proven on different samples.  
36  
37  
38

39  
40 (2) Samples were continuously heated to the annealing temperature and the heat  
41 release during this heating ( $\delta H_1$ ) was measured, Fig. 1b. The samples were  
42 annealed at different temperatures for 1h and then cooled down to 323 K.  
43  
44  
45  
46

47  
48 (3) Finally the same samples used in the respective second step were heated from  
49 323 K to 723 K and the heat release ( $\delta H_2$ ) during this scan was measured,  
50 Fig. 1b.  
51  
52  
53  
54  
55

56 For each sample, two identical DSC runs were carried out. The second run was used  
57 as a baseline, which was then subtracted from the first run to obtain the irreversible  
58  
59  
60

1  
2  
3 part of the measurement signal and thus to remove the device function from the  
4  
5 analysis.  
6  
7

8  
9 In order to monitor the microstructural evolution, X-ray diffraction was performed  
10  
11 subsequently using a Siemens D5000 diffractometer with  $\text{CuK}\alpha$  radiation  
12  
13 ( $\lambda = 1.5406 \text{ \AA}$ ) operating at 40 kV and 40 mA. These XRD spectra were recorded in  
14  
15 the  $2\theta$  range from  $25^\circ$  to  $90^\circ$  with a scan speed of  $0.2^\circ/\text{min}$  and increments of  $0.02^\circ$ .  
16  
17

18  
19 The TEM measurements were performed on as-prepared and thermally treated  
20  
21 samples using a Libra FE200 and a Tecnai F20, transmission electron microscope.  
22  
23 Specimens for transmission electron microscopy (TEM) were prepared by  
24  
25 electropolishing using a solution of  $\text{HNO}_3$  (65%) and  $\text{CH}_3\text{OH}$  in the ratio of 1:2 by  
26  
27 volume. The electrolyte was cooled to  $-20^\circ\text{C}$  and the voltage applied for thinning  
28  
29 was 10 V. Note that the selected area electron diffraction (SAED) images recorded on  
30  
31 the Libra FE200 microscope contain artificial features due to the switching of the  
32  
33 mechanical shutter when ultra-short exposure times were used for the CCD-camera.  
34  
35 This is a machine-related problem and can not be completely avoided. However the  
36  
37 artifacts do not corroborate the diffraction pattern and thus main message of SAED  
38  
39 images is clearly seen and is not affected by these artifacts.  
40  
41  
42  
43  
44

### 45 **3. Results**

#### 46 **3.1 TEM**

47  
48  
49 The as-prepared samples consist of both a minority nanocrystalline and a majority  
50  
51 amorphous phase after HPT, where the structure of the crystalline fraction  
52  
53 corresponds to the austenite (B2) phase, Fig 2a. The size of the nanocrystalline grains  
54  
55 is extremely small with average diameters of about 5-15 nm. The samples were heated  
56  
57 to the given maximum temperature in the range of 453 K to 723 K with a heating rate  
58  
59  
60

1  
2  
3 of 10 K/min and cooled down with a cooling rate of 100 K/min. The corresponding  
4 microstructures that developed during these thermal treatments are shown in Fig. 2.  
5  
6 These heating temperatures were chosen to analyze the microstructural evolution  
7 during the DSC scan shown in Fig. 1a. The samples are partially crystalline after  
8 heating to 453 K; also several amorphous bands are visible. On increasing the  
9 maximum temperature, the crystalline fraction is increasing and one can easily  
10 distinguish the crystalline and amorphous regions of the samples, as shown in the  
11 diffraction patterns of region A and B after heating to 563 K (Fig. 2d). There is no  
12 sign of grain growth and amorphous bands are clearly visible in the sample heated up  
13 to 563 K. Though the material appears to be completely crystalline after heating to  
14 623 K, a narrow region of amorphous contrast still exists as shown in Fig. 2e. The  
15 diffraction pattern of this narrow region is not clearly amorphous, because the  
16 selected area aperture covered the crystalline area as well. After heating the sample to  
17 the maximum temperature of 723 K, the sample is completely crystalline and shows  
18 clearly visible grains with an average size of about 30 nm. This result shows that there  
19 is grain growth in the material at temperatures above 623 K.  
20  
21  
22  
23  
24  
25  
26  
27  
28  
29  
30  
31  
32  
33  
34  
35  
36  
37  
38  
39  
40

41 A different set of samples was annealed in the DSC for 1 h at different temperatures  
42 in the range of 453 K to 723 K following heating with the rate of 10 K/min.  
43 Afterwards, the microstructures of these samples were analyzed by TEM. Fig. 3a-b  
44 show that after annealing at 373 K and 453 K, the crystalline fraction is increased  
45 compared to the as-prepared specimen at RT (Fig. 2a) but still a significant  
46 amorphous fraction existed, as verified by the diffuse halo of the diffraction pattern.  
47  
48 The diffraction patterns obtained on the samples after annealing at even higher  
49 temperatures indicates that the sample is mostly crystalline after annealing at 523 K,  
50 although the bright field TEM image looks similar as the one obtained after annealing  
51  
52  
53  
54  
55  
56  
57  
58  
59  
60

1  
2  
3 at 453 K. These results indicate that a small amorphous fraction is difficult to quantify  
4  
5 from diffraction results. Further annealing at 723 K shows that the sample is not only  
6  
7 completely crystalline but that there are clearly visible grains of an average size about  
8  
9 40 nm. A large variation in the grain size is observed after annealing at 723 K. Some  
10  
11 grains have anomalously large sizes of about 120 nm.  
12  
13

### 14 15 16 **3.2 DSC and XRD**

17  
18 A typical calorimetric signal measured on as-deformed nano-NiTi is shown in Fig. 1a.  
19  
20 Two exothermic processes can be distinguished; one starts at about 373 K and the  
21  
22 second starts at 573 K with a peak heat release at 626 K (at a heating rate of  
23  
24 10 K/min), (Fig. 1a). A set of isothermal treatments (Fig. 4) always using the same  
25  
26 specimen has been done by heating the sample with a constant heating rate of  
27  
28 10 K/min to sequentially higher temperatures ranging from 453 K to 723 K followed  
29  
30 by isothermal holding for 1 h at each annealing temperature. There is an exothermic  
31  
32 event on the signal during the first heating run to 453 K, where the area of this peak  
33  
34 corresponds to the enthalpy  $\delta H_1 = 3.4$  J/g. This exothermic peak is related to stress  
35  
36 relaxation and the onset of the crystallization, as confirmed by the DSC scan in Fig. 4  
37  
38 and the TEM image shown in Fig. 2b.  
39  
40  
41  
42  
43

44  
45 The XRD spectra of as-prepared specimen (Fig. 5), indicate a shoulder peak at  
46  
47  $2\theta = 39.8^\circ$  along with the peak corresponding to the partially amorphous phase at  
48  
49  $2\theta = 42.3^\circ$ . The TEM examinations of Fig. 2 and Fig. 3 show the clear absence of the  
50  
51 R- or B19' phase. A layered structure consisting of neighboring bands of amorphous  
52  
53 and partially crystalline phases is observed too, – a finding is consistent with the  
54  
55 results of Peterlechner et al. [28]. **Based on these findings, we may suggest that the**  
56  
57 **shoulder peak corresponds to a (deformed or strained) B2 NiTi phase appearing as**  
58  
59 **separate bands in the microstructure.** The corresponding difference in the lattice  
60

constants of the B2 NiTi phases corresponding to the angular difference between the shoulder peak and the main peak,  $\Delta a$ , is 0.1882 Å. The alternating thin layers of the B2 phase with different lattice parameters produce locally a bi-axial stress with a maximum value,  $\sigma$ , that can be estimated as:

$$\sigma = \frac{E}{1-\nu} \times \frac{\Delta a}{a} \quad (2)$$

where  $E$  is the Young modulus,  $\nu$  is the Poisson ratio. Taking Young's modulus of the NiTi alloy as 49 GPa [29], the maximum residual stress in the alloy is estimated as 4 GPa that is a reasonable value for a sample deformed at 5 GPa. The reduced heat required to relax this stress,  $U$ , is 1.38 J/g, calculated as:

$$U = \frac{1}{2} \sigma \frac{\Delta a}{a} \times \frac{1}{\rho} \quad (3)$$

Here,  $\rho$  is the density of the NiTi alloy. This estimation fits reasonably the DSC measurement (the heat release is obtained as:  $\delta H_1 = 3.4$  J/g, during heating to 453 K, Fig. 4). Therefore, we conclude that heating to 453 K results in a degeneracy of the shoulder peak and is probably related to the recovery of residual stresses in the HPT-deformed samples. By the observation of other DSC scans for heating to the temperatures between 523 K to 723 K, followed by annealing at each temperature for 1 h, it is clear (Fig. 4) that these curves are quite flat and the onset temperature of the exothermic signals are at 493 K, 553 K and 573 K, when the sample was heated to the maximum temperatures 523 K, 563 K and 623 K, respectively. At the higher temperatures no signal is measured after further annealing at 723 K. A large exothermic signal is observed on heating the specimen to 575 K.

A further calorimetric analysis has been done to explain the crystallization kinetics during isothermal annealing. Since the signal is rather weak, develops sluggishly and

1  
2  
3 since the calorimetric sensitivity is proportional to the heating rate, direct  
4 determination during the isothermal annealing is not sufficiently accurate. To estimate  
5 the heat release  $\delta H$  during isothermal annealing,  $\delta H_{\text{total}}$ ,  $\delta H_1$  and  $\delta H_2$  were measured  
6 for the annealing treatment at different temperatures ranging from 453 K to 723 K and  
7 these values are shown in Fig. 6.  $\delta H$  is calculated in the following way:

$$\delta H = \delta H_{\text{total}} - (\delta H_1 + \delta H_2) \quad (4)$$

18  $\delta H_{\text{total}}$  is the heat release during heating of the sample from 323 K to 723 K and has  
19 the constant value  $38.62 \pm 1.78$  J/g. The heat release during continuous heating up to  
20 the annealing temperature,  $\delta H_1$ , was measured and samples were annealed for 1 h at  
21 the final temperatures in the range from 453 K to 723 K. After that the same sample  
22 was continuously heated from 323 K to 723 K and the heat release during this heating,  
23  $\delta H_2$ , was measured. Thus the heat release during isothermal annealing,  $\delta H$ , is  
24 calculated using Eq. 4. The values of  $\delta H$ ,  $\delta H_1$  and  $\delta H_2$  are plotted in Fig. 6 as a  
25 function of the isothermal annealing temperature. The data obtained from this analysis  
26 shows an unexpected but reproducible tendency: the value of  $\delta H$  decreases at  $T_A =$   
27 523 K due to the increase in the value of  $\delta H_2$ . This experimental result thus means  
28 that the crystalline fraction decreases with increasing temperature.

29 The XRD spectra after each annealing treatment in the DSC are shown in Fig. 5.  
30 These XRD spectra were recorded on the same sample used for the DSC  
31 measurements (sample used for Fig. 4) during annealing in order to achieve maximum  
32 comparability between calorimetry and X-ray diffraction results. The as-prepared  
33 specimen reveals a disordered structure at room temperature with a very broad peak  
34 corresponding to the amorphous phase, centered at  $2\theta = 42.3^\circ$  including the small  
35 peak at  $2\theta = 39.8^\circ$ . Similar to the result obtained after annealing at 453 K a broad  
36 peak was observed at  $2\theta = 42^\circ$ . This less broad peak indicates that on annealing at 453

1  
2  
3  
4  
5  
6  
7  
8  
9  
10  
11  
12  
13  
14  
15  
16  
17  
18  
19  
20  
21  
22  
23  
24  
25  
26  
27  
28  
29  
30  
31  
32  
33  
34  
35  
36  
37  
38  
39  
40  
41  
42  
43  
44  
45  
46  
47  
48  
49  
50  
51  
52  
53  
54  
55  
56  
57  
58  
59  
60

K the stress present in the NiTi alloy has relaxed but the material still consists mostly of the amorphous phase. The spectra recorded after annealing at higher temperatures show that the material is mostly crystalline after annealing at 563 K while the sharpest peak observed after annealing at 723 K support the result obtained by the TEM and DSC observations. The peaks were identified as the (110), (200) peaks (211) of the austenite (B2) phase. To calculate the grain size of the NiTi alloy, Scherrer's formula [30] has been used, assuming that there is no strain in the material after annealing at 453 K,

$$D_v = \frac{K\lambda}{\{\beta \cos\theta\}} \quad (5)$$

$$\text{and } \beta = (\beta_{\text{obs}}^2 - \beta_{\text{inst}}^2)^{1/2}$$

Where  $\beta$  is the integral width (in radians  $2\theta$ ) of the reflection located at  $2\theta$ ,  $\beta_{\text{inst}} = 0.134$  and  $\beta_{\text{obs}}$  is the integral width calculated by XRD data (Fig. 5) at different temperatures,  $D_v$  is the volume weighted crystallite size and  $K$  is the Scherrer constant with a value in the range of 0.87 – 1.0. In the present study,  $K$  has been chosen as unity,  $\lambda$  is the wavelength of the radiation with a value of 1.54 Å. The grain sizes of the crystallites are listed in Table 1 together with the respective annealing temperatures.

#### 4. Discussion

It is well known that NiTi is susceptible to amorphization as a result of various processing treatments and the formation of an amorphous phase was detected, for example in the case of ion beam mixing [31], mechanical alloying [32], ion implantation [33], shot peening [34], as well as cold rolling [24, 26, 35, 36] and shear deformation [37]. However in these publications the amorphization of NiTi was

1  
2  
3 observed on the surface or as discrete amorphous bands within a crystalline matrix. In  
4  
5 this investigation similar to earlier studies [12] we demonstrate the formation of bulk  
6  
7 amorphous NiTi alloy by HPT and the formation of a homogenous nanostructure by  
8  
9 its crystallization and growth under controlled heating and annealing conditions. The  
10  
11 as-deformed NiTi alloy was partially amorphous, with nanocrystals of extremely  
12  
13 small sizes of 5-15 nm in diameter (Fig. 2a). This feature is also reported by  
14  
15 Sergueeva et al. [12]. Fig. 2 shows the amorphous bands after heating to 453 K and  
16  
17 523 K, these bands are probably connected with deformation localization in the shear  
18  
19 bands. The electron diffraction pattern made from an amorphous-nanocrystalline area  
20  
21 (Fig. 2d) demonstrates the presence of the amorphous phase halo and extended  
22  
23 reflexes from the nanocrystalline B2 phase. Peterlechner et al. [28] have also reported  
24  
25 the presence of well-defined interfaces of amorphous bands with respect to the  
26  
27 nanocrystalline phase in the cross-section of HPT-deformed NiTi, while in case of the  
28  
29 plane-section, the amorphous phase is obscured by overlapping nanograins in the  
30  
31 TEM projection. In the present study, the amorphous bands in the plane-section are  
32  
33 well-defined and straight interfaces with respect to the nanocrystalline phase (Fig.  
34  
35 2b).

36  
37 The data analyzed in Fig. 6 shows an unexpected but reproducible tendency: the value  
38  
39 of  $\delta H$  decreases at  $T_A = 523$  K due to the increase of the value of  $\delta H_2$ . It is obvious,  
40  
41 that this signature of the enthalpy release cannot be explained by nucleation and  
42  
43 growth transformations, since these processes are monotonous in temperature. The  
44  
45 possible cause of this unusual decrease in  $\delta H$  is a reverse amorphization during  
46  
47 annealing at 523 K. The microstructure in Fig. 2c shows amorphous bands between  
48  
49 the crystalline regions. These amorphous bands are the region of deformation  
50  
51 localization where the highest defect densities were created. The crystals which are  
52  
53  
54  
55  
56  
57  
58  
59  
60

1  
2  
3 situated at these boundaries of the crystalline and the amorphous regions have more  
4 defects and a more disorders interface and are hence in an energetically more unstable  
5 state. Thus annealing at 523 K might trigger them to transform thermally into an  
6 amorphous state, as in this state half of the interface energy is saved as compared to  
7 the nanocrystalline state. The excess free energy densities due to the interface might  
8 have the effect of raising the free energy of the crystal to a level above that of the  
9 amorphous phase according to Koike et al. [35]. In addition, defects, especially  
10 dislocations, are transformed or completely annihilated upon amorphization  
11 consequently, due to the higher amorphous fraction after annealing at 523 K, there is  
12 an unusual increase in  $\delta H_2$  (heat release during continuous heating from 323 K to 723  
13 K after annealing at 523 K) and a corresponding decrease in  $\delta H$ . The value of  $\delta H$  at  $T_A$   
14 = 453 K is higher than the value obtained after annealing at  $T_A = 563$  K and 623 K  
15 due to the stress relaxation in addition to crystallization. It also implies that the  
16 annealing treatment induced crystallization at lower temperatures and grain growth at  
17 higher temperatures, this explanation is also supported by the TEM data shown in  
18 Fig. 3. The large variation in the grain size after annealing at 723 K, (Fig. 3d and 3e)  
19 shows that these grains are most probably those grains, which were already present  
20 after HPT deformation and became large during the annealing treatment. The results  
21 indicate that crystallization occurs by nucleation of new crystals and the rate of  
22 volume transformation due to nucleation is faster than the growth rate of pre-existing  
23 nanocrystals [38] at lower temperatures, while at higher temperatures grain growth of  
24 newly formed crystals and preexisting nanocrystals takes place simultaneously.

25  
26  
27  
28  
29  
30  
31  
32  
33  
34  
35  
36  
37  
38  
39  
40  
41  
42  
43  
44  
45  
46  
47  
48  
49  
50  
51  
52  
53  
54  
55  
56  
57  
58  
59  
60  
The grain sizes mentioned in Table 1, after annealing at 523 K and 723 K were used  
to estimate the decrease of the grain boundary energy after heating to temperatures  
above 523 K to 723 K (Fig. 7) by using the equation:

$$\frac{\Delta H}{m} = \frac{\Delta A \cdot \gamma}{\rho \cdot V} \quad (7)$$

Here,  $A = \frac{2.91 \cdot V}{d}$  is the average surface area of the GBs in a polycrystal with a given grain size,  $d$ . Here  $\Delta H/m$  is the heat release per unit weight,  $\gamma$  is the grain boundary energy,  $\Delta A$  is change in the GB area,  $V$  is the volume and  $\rho$  is the density of the material. The calorimetric estimation of the grain boundary energy by Eq. 7 is 0.66 J/m<sup>2</sup> which is in good agreement with the grain boundary energy of 0.49 J/m<sup>2</sup> estimated in the literature by using Borisov's analysis [39] in case of NiTi [40-42] for the same temperatures as used in the present study. The details of Borisov's analysis are well explained in reference [43]. Although this value presents a rough estimate, it supports the interpretation that the main peak observed in the DSC scan (Fig. 1a) is related to the grain growth of the material. Thus the initial exothermic signal present in the DSC scan at temperatures below 573 K shown in Fig.4 corresponds to the relaxation of the stress created by HPT and the crystallization of the material. The TEM image in Fig. 2e shows the existence of a mainly crystalline microstructure along with a small amorphous fraction. It indicates that the most intense peak in the DSC scan in Fig. 1a is related mainly to grain growth as well as the crystallization of the residual amorphous part. Thus the activation energy estimated in the present study is a convolution of the activation energy of grain growth and crystallization of the residual amorphous part. The activation energy of crystallization is expected to be low in the present case, since the temperature  $T_P$  obtained in the present case of HPT deformed NiTi is almost 150 K lower than  $T_P$  of crystallization measured on thin amorphous ribbons of NiTi obtained by melt spinning (MS) or sputter deposition (SD), with peak temperatures between about 773 K and 833 K [19, 21-22]. This result indicates a lower thermal stability of the amorphous phase obtained by HPT in the

1  
2  
3 present study as compared to the previously reported data on NiTi amorphized by  
4 different techniques. These differences might be caused by different structures of the  
5 amorphous phase in the as-deformed material: NiTi made amorphous by HPT  
6 contains nanocrystalline debris that can act as nucleation sites or nucleation  
7 “embryos” with sizes that are smaller than the critical radius for nucleation. Their  
8 presence could lower the energy barrier for forming a critical nucleus [44] and the  
9 corresponding activation energy of crystallization. This nanocrystalline debris along  
10 with nanocrystals is not found in the amorphous phase of NiTi obtained by SD or MS  
11 [38].  
12  
13  
14  
15  
16  
17  
18  
19  
20  
21  
22  
23  
24

## 25 **5. Summary**

26  
27  
28 Homogenous nanocrystalline material with different grain size has been obtained by  
29 nanocrystallization of an amorphous phase using controlled annealing. Both the  
30 thermal stability and the crystallization kinetics of HPT-processed amorphous NiTi  
31 differ considerably from those reported in previous studies. One can tailor the  
32 properties of NiTi by obtaining the nanocrystalline structure, depending on the degree  
33 of the deformation and the temperature of the subsequent annealing treatments.  
34 Additionally, the experimentally observed values of the enthalpy release and of the  
35 crystalline fraction as functions of the annealing temperature clearly show that they  
36 cannot be explained by a nucleation and growth process. In fact, the reproducible data  
37 obtained here can be consistently explained by suggesting a reverse amorphization  
38 process in the HPT-deformed NiTi during annealing at 523 K for 1 h. The large  
39 variability of the structural response of the material upon thermal or thermomechanical  
40 treatment explains the large range of reported structures of this class of alloys. At the  
41 same time, these results indicate the large potential for microstructure tailoring that is  
42 offered by the delicate balance between nucleation, grain growth and amorphization.  
43  
44  
45  
46  
47  
48  
49  
50  
51  
52  
53  
54  
55  
56  
57  
58  
59  
60

## Acknowledgement

Financial support by the Deutsche Forschungsgemeinschaft (DFG) is gratefully acknowledged. The authors also acknowledge the support from the Russian Foundation for Basic Research (project number 08-02-91955).

## Reference

- [1] S. Turenne, S. Prokoshkin, V. Brailovski, N. Sacepe, *Can. Metall. Quart.* 39 (2000) p. 217.
- [2] A. Kapanen, J. Ilvesaro, A. Danilov, J. Ryhanen, P. Lehenkari, J. Tuukkanen, *Biomaterials* 23 (2002) p. 645.
- [3] R. Hernandez, S. Polizu, S. Turenne, L'H. Yahia, *Bio-med. Mater. Eng.* 12 (2002) p. 37.
- [4] P. Filip, J. Musialek, H. Lorethova, J. Nieslanik, K. Mazanec, *J. Mater. Sci. Mater. Med.* 7 (1996) p. 657.
- [5] B.Y. Li, L.J. Rong, Y.Y. Li, V.E. Gjunter, *Scripta Mater.* 44 (2001) p. 823.
- [6] D. Mantovani, *JOM* October (2006) p. 36.
- [7] W.J. Moberly and K.N. Melton, *Engineering Aspects of Shape Memory Alloys*, Butterworth-Heinemann Ltd. Boston (1990) p. 46.
- [8] R. Birringer, H. Gleiter, H.P. Klein, P. Marquardt, *Phys. Lett.* 102A (1984) p. 365.
- [9] R.Z. Valiev, *Nat. Mater.* 3 (2004) p. 511.
- [10] V.G. Pushin, V.V. Stolyarov, R.Z. Valiev, T.C. Lowe, Y.T. Zhu, *Mater. Sci. Eng. A* 410 (2005) p. 386.

- 1  
2  
3  
4 [11] R.Z. Valiev, R.K. Islamgaliev, I.V. Alexandrov, *Prog. Mater. Sci.* 45 (2000) p.  
5 103.  
6  
7  
8  
9 [12] A.V. Sergueeva, C. Song, R.Z. Valiev, A.K. Mukherjee, *Mater. Sci. Eng. A*  
10 339 (2003) p. 159.  
11  
12  
13  
14 [13] T. Waitz, V. Kazykhanov, H.P. Karnthaler, *Acta Mater.* 52 (2004) p. 137.  
15  
16  
17 [14] J.Y. Huang, Y.T. Zhu, X.Z. Liao, R.Z. Valiev, *Philos. Mag. Lett.* 84 (2004) p.  
18 183.  
19  
20  
21  
22 [15] T. Waitz, *Acta Mater.* 53 (2005) p. 2273.  
23  
24  
25 [16] T. Waitz, T. Antretter, F.D. Fischer, N.K. Simha, H.P. Karnthaler, *J. Mech.*  
26 *Phys. Solids* 55 (2007) p. 419.  
27  
28  
29  
30 [17] H.-J. Lee, A.G. Ramirez, *Appl. Phys. Lett.* 85 (2004) p. 1146.  
31  
32  
33 [18] H.-J. Lee, h. Ni, D.T. Wu, A.G. Ramirez, *Mater. Trans.* 47 (2006) p. 527.  
34  
35  
36 [19] X. Wang, J.J. Vlassak, *Scripta Mater.* 54 (2006) p. 925.  
37  
38  
39 [20] K.T. Liu, J.G. Duh, *J. Non-Cryst. Solids* 353 (2007) p. 1060.  
40  
41  
42 [21] K.H.J. Buschow, *J. Phys. F: Met. Phys.* 13 (1983) p. 563.  
43  
44  
45 [22] S.H. Chang, S.K. Wu, H. Kimura, *Intermetallics* 15 (2007) p. 233.  
46  
47  
48 [23] D.V. Louzguine, A. Inoue, *J. Mater. Sci.* 35 (2000) p. 4159.  
49  
50  
51 [24] N.M. Matveeva, Y.K. Kovneristy, Y.K. Bykovsky, A.V. Shelyakov, O.V.  
52 Kostyanaya, *Izv. Akad. Nauk. SSSR Metall.* 4 (1989) p. 171.  
53  
54  
55 [25] G.P. Dinda, R. Rösner, G. Wilde, *Ultrafine Grained Materials III*, TMS (2004)  
56 p. 309.  
57  
58  
59  
60

- 1  
2  
3 [26] G.P. Dinda, R. Rösner, G. Wilde, *Solid State Phenomena* 101-102 (2005) p.  
4  
5 55.  
6  
7  
8  
9 [27] M. Peterlechner, T. Waitz, H.P. Karnthaler, in: proceedings of the  
10  
11 International Symposium on Bulk Nanostructured Materials, Ufa, Russia,  
12  
13 2007, p. 57.  
14  
15  
16 [28] E. Wibowo and C. Y. Kwok, *J. Micromech. Microeng.* 16 (2006) p. 101.  
17  
18  
19 [29] A.L. Patterson, *Phys. Rev.* 56 (1939) p. 978.  
20  
21  
22 [30] B.X. Liu, W.L. Johnson, M.A. Nicolet, *Appl. Phys. Lett.* 42 (1983) p. 45.  
23  
24  
25 [31] R.B. Schwarz, R.R. Petrich, C.K. Saw, *J. Non-Cryst. Solids* 76 (1985) p. 281.  
26  
27  
28 [32] P. Moine, O. Popoola, J.P. Villain, *Scripta Metall.* 20 (1986) p. 305.  
29  
30  
31 [33] D.M. Grant, S.M. Green, J.V. Wood, *Acta Metall. Mater.* 43 (1995) p. 1045.  
32  
33  
34 [34] J. Koike, D.M. Parkin, M. Nastasi, *J. Mater. Res.* 5 (1990) p. 1414.  
35  
36  
37 [35] H. Nakayma, K. Tsuchiya, M. Umemoto, *Scripta Mater.* 44 (2001) p. 1781.  
38  
39  
40 [36] Y.E. Tat'yanin, V.G. Kurdyumov, V.B. Fedorov, *Phys. Met. Metall.* 62 (1990)  
41  
42 p. 257.  
43  
44  
45 [37] M. Peterlechner, T. Waitz, H.P. Karnthaler, *Scripta Mater.* 60 (2009) p. 1137.  
46  
47  
48 [38] M. Peterlechner, T. Waitz, H.P. Karnthaler, *Scripta Mater.* 59 (2008) p. 566.  
49  
50  
51 [39] V.T. Borisov, V.T. Golikov, G.V. Shcherbedinsky, *Phys. Metall. Metallogr.*  
52  
53 17 (1964) p. 881.  
54  
55  
56 [40] S.V. Divinski, I. Stloukal, L. Kral, Chr. Herzig, *Defect and Diffusion Forum*  
57  
58 289-292 (2009) p. 377.  
59  
60

- 1  
2  
3  
4 [41] J. Bernardini, C. Lexcellent, L. Daróczy and D.L. Beke, Philo. Mag. 83 (2003)  
5 p. 329.  
6  
7  
8  
9 [42] A.M. Kalinina, V.N. Filipovich, G.A. Sycheva, J. Non-Cryst. Solids 219  
10 (1997) p. 80.  
11  
12  
13  
14 [43] S.V. Divinski, G. Reglitz, G. Wilde, Acta Mater. 58 (2010) p. 386.  
15  
16  
17 [44] A.M. Kalinina, V.N. Filipovich, G.A. Sycheva, J. Non-Cryst. Solids 219  
18 (1997) p. 80.  
19  
20  
21  
22  
23  
24  
25  
26  
27  
28  
29  
30  
31  
32  
33  
34  
35  
36  
37  
38  
39  
40  
41  
42  
43  
44  
45  
46  
47  
48  
49  
50  
51  
52  
53  
54  
55  
56  
57  
58  
59  
60

1  
2  
3  
4  
5  
6  
7  
8  
9  
10  
11  
12  
13  
14  
15  
16  
17  
18  
19  
20  
21  
22  
23  
24  
25  
26  
27  
28  
29  
30  
31  
32  
33  
34  
35  
36  
37  
38  
39  
40  
41  
42  
43  
44  
45  
46  
47  
48  
49  
50  
51  
52  
53  
54  
55  
56  
57  
58  
59  
60

Temperature (K)	453	523	563	623	723
Grain size (nm)	3	5	9	13	20

Table 1. Grain size of NiTi alloy after annealing at different temperature estimated by Scherrer formula.

For Peer Review Only

**Figure captions:**

Figure 1. DSC curve for continuous heating from 323 K to 723 K using a heating rate of 10 K/min, (a)  $\Delta H_{\text{total}}$ , and DSC signals step-wise annealing treatment (b) continuous heating from 323 K to 563 K is  $\Delta H_1$ , annealing for 1 h at 563 K followed by cooling down to 323 K and the same sample was continuously heating from 323 K to 723 K,  $\Delta H_2$ . The DSC scan curve for  $\Delta H_2$  is shifted for convenient comparison.

Figure 2. Microstructure evolution of the NiTi alloy after heating to different temperatures.

Figure 3. Microstructure evolution of the NiTi alloy after annealing for 1 h at different temperatures.

Figure 4. The heat release by continuous heating of the NiTi alloy using the same sample to different maximum temperatures. The heating rate was always 10 K/min and the sample has subsequently been annealed for 1 h at each temperature.

Figure 5. X-ray diffractograms showing the structure of the NiTi alloy before and after annealing at different temperatures for 1 h.

Figure 6. Heat release vs. temperature (heating rate 10 K/min and annealed for 1 h at each temperature). Symbols are explained in the experimental details section.

Figure 7. Heat release during continuous heating from 523 K to 723 K.

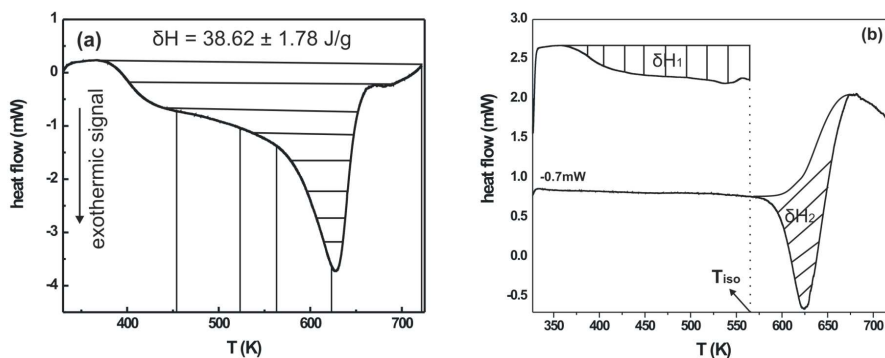


Figure 1. DSC curve for continuous heating from 323 K to 723 K using a heating rate of 10 K/min, (a)  $\Delta H_{total}$ , and DSC signals step-wise annealing treatment (b) continuous heating from 323 K to 563 K is  $\Delta H_1$ , annealing for 1 h at 563 K followed by cooling down to 323 K and the same sample was continuously heating from 323 K to 723 K,  $\Delta H_2$ . The DSC scan curve for  $\Delta H_2$  is shifted for convenient comparison.

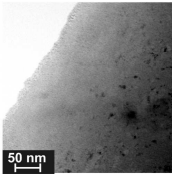
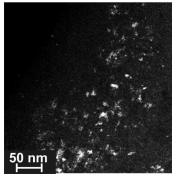
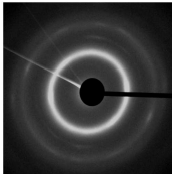
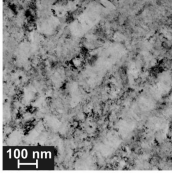
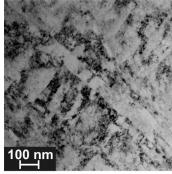
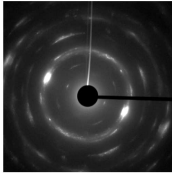
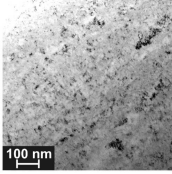
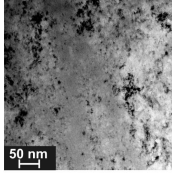
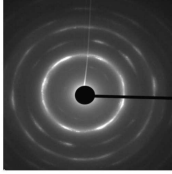
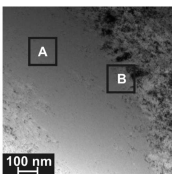
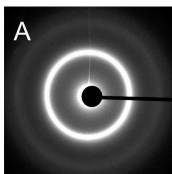
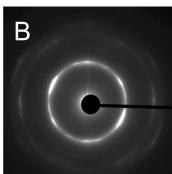
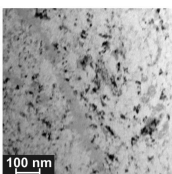
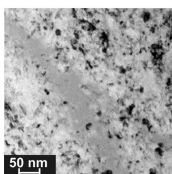
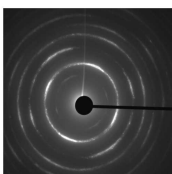
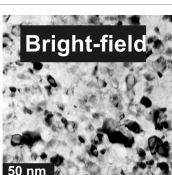
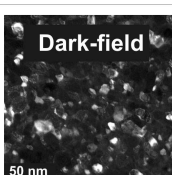
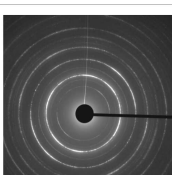
S.N.	T(K)			SAED
a	As-prepared			
b	453			
c	523			
d	563			
e	623			
f	723			

Figure 2. Microstructure evolution of the NiTi alloy after heating to different temperatures.

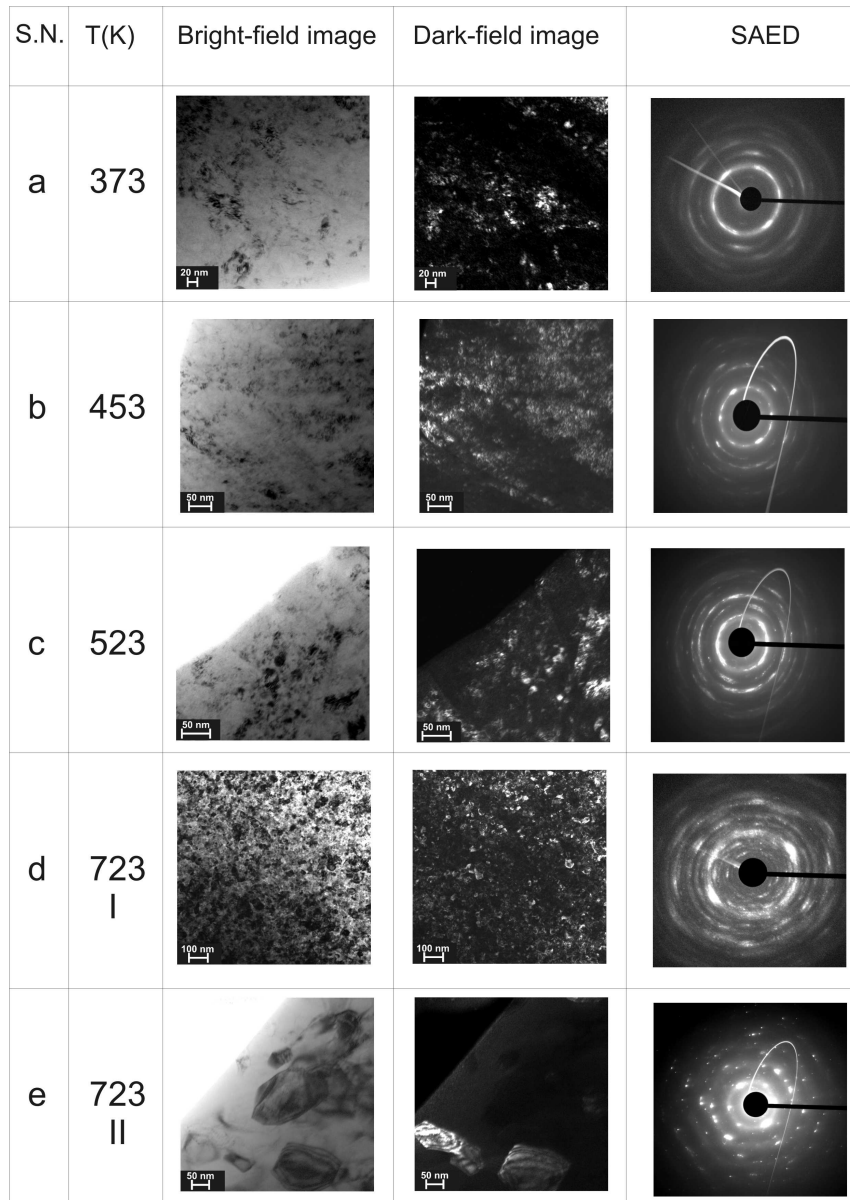


Figure 3. Microstructure evolution of the NiTi alloy after annealing for 1 h at different temperatures.

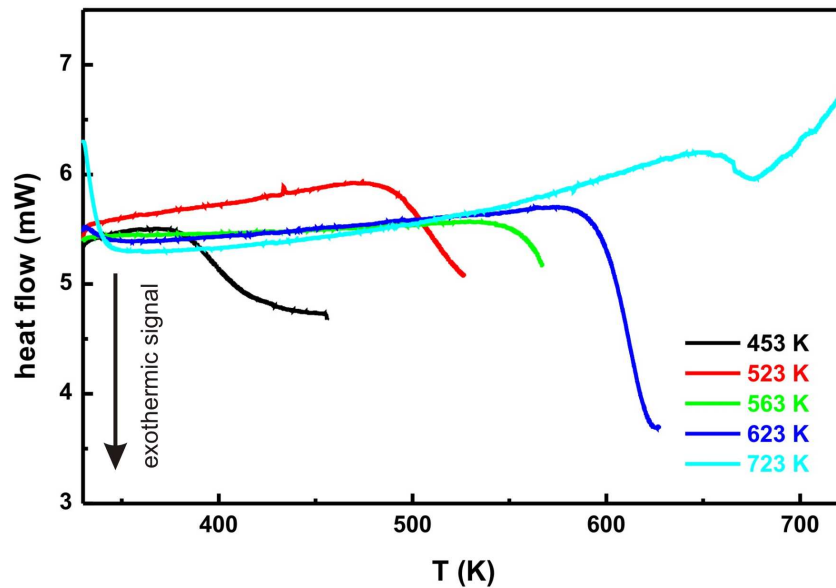


Figure 4. The heat release by continuous heating of the NiTi alloy using the same sample to different maximum temperatures. The heating rate was always 10 K/min and the sample has subsequently been annealed for 1 h at each temperature.  
177x123mm (300 x 300 DPI)

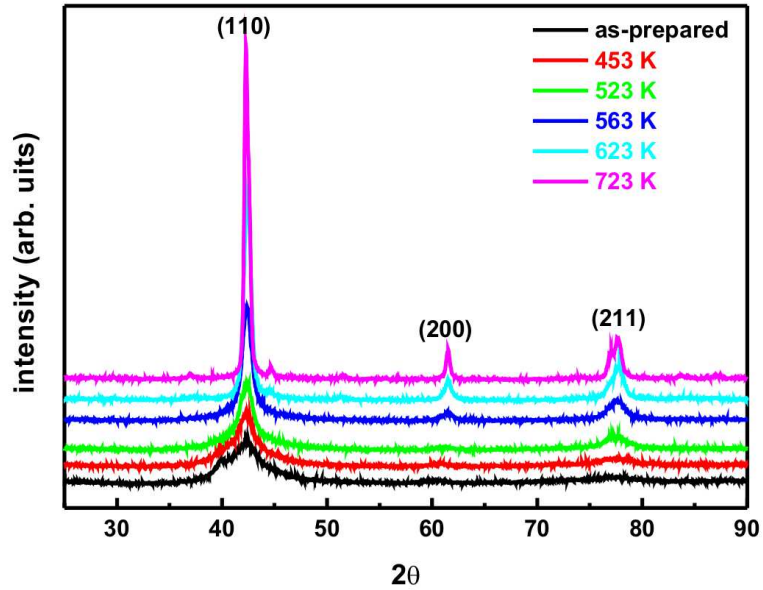


Figure 5. X-ray diffractograms showing the structure of the NiTi alloy before and after annealing at different temperatures for 1 h  
115x80mm (300 x 300 DPI)

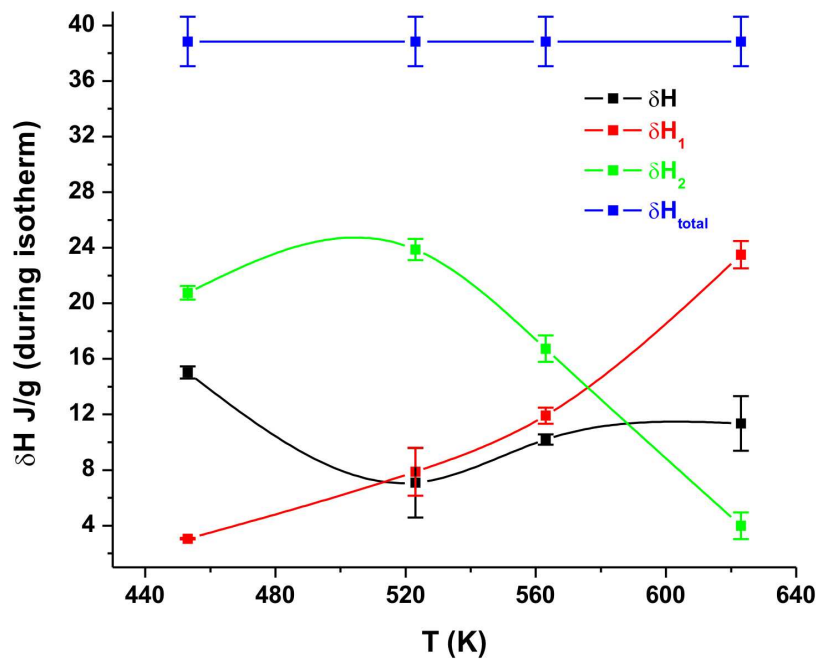


Figure 6. Heat release vs. temperature (heating rate 10 K/min and annealed for 1 h at each temperature). Symbols are explained in the experimental details section.  
152x118mm (300 x 300 DPI)

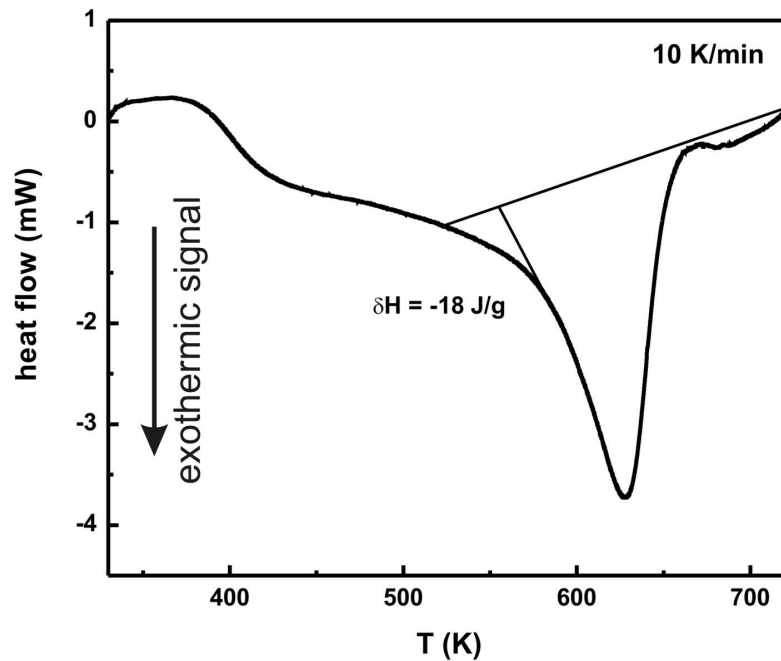


Figure 7. Heat release during continuous heating from 523 K to 723 K.  
152x117mm (300 x 300 DPI)

Temperature (K)	453	523	563	623	723
Grain size (nm)	3	5	9	13	20

For Peer Review Only